ACSNANO
www.acsnano.org
ARTICLE

Observing and Controlling the Folding Pathway of DNA Origami at the Nanoscale

Jonathan Lee Tin Wah,[†,‡] Christophe David,[§] Sergii Rudiuk,[⊥,∥,#] Damien Baigl,[⊥,∥,#] and André Estevez-Torres*[,†,‡]

[†]Laboratoire Jean Perrin, Université Pierre et Marie Curie, 4 place Jussieu, 75005 Paris, France
[‡]CNRS, UMR 8237, 75005 Paris, France
[§]Laboratoire de photonique et de nanostructures, CNRS, route de Nozay, 91460 Marcoussis, France
[⊥]Department of Chemistry, Ecole Normale Supérieure−PSL Research University, 24 Rue Lhomond, 75005 Paris, France
[∥]Sorbonne Universités, UPMC Univ Paris 06, PASTEUR, 75005 Paris, France
[#]CNRS, UMR 8640 PASTEUR, 75005 Paris, France

Supporting Information

ABSTRACT: **DNA origami is a powerful method to fold DNA into rationally designed nanostructures that holds great promise for bionanotechnology. However, the folding mechanism has yet to be fully resolved, principally due to a lack of data with single molecule resolution. To address this issue, we have investigated in detail, using atomic force microscopy, the morphological evolution of hundreds of individual rectangular origamis in solution as a function of temperature. Significant structural changes were observed between 65 and 55 °C both for folding and melting, and six structural intermediates were identified. Under standard conditions, folding was initiated at the edges of the rectangle and progressed toward the center. Melting occurred through the reverse pathway until the structures were significantly disrupted but ended through a different pathway involving out-of-equilibrium chainlike structures. Increasing the relative concentration of center to edge staples dramatically modified the folding pathway to a mechanism progressing from the center toward the edges. These results indicate that the folding pathway is determined by thermodynamics and suggest a way of controlling it.**

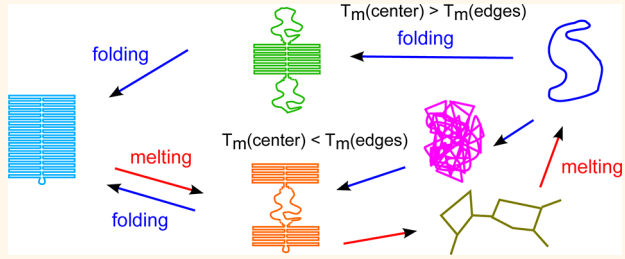

KEYWORDS: *DNA nanotechnology, AFM, image processing, nanostructure*

Structural DNA nanotechnology designs nanostructures using DNA strands as building blocks.[1−5] In contrast with standard top-down fabrication techniques, such as lithography, it is a bottom-up process: billions of DNA strands are mixed in a water solution and self-assemble into the final nanostructures. DNA building blocks are particularly advantageous because the self-assembly rules are simple and relatively robust, with Watson−Crick pairing as the principal rule.

A small revolution happened in the field when Rothemund invented DNA origami:[3] mixing a 7249 bases-long single-stranded DNA (ssDNA), the scaffold, with a set of well-designed oligonucleotides, about 32 bases long, the staples, allowed the fabrication of arbitrary two-dimensional shapes about 100 nm across. Later, three-dimensional structures could also be obtained following a similar principle.[6−8] Recently, Yin and co-workers introduced single-stranded tile assembly, where arbitrary 2D and 3D structures were self-assembled from oligonucleotides alone.[26] Hollow 3D structures were also obtained by designing new scaffolds using surface rendering principles.[10]

Since the advent of DNA origami almost a decade ago, the progress of DNA nanotechnology has been enormous as attested by the incipient applications of this technique,[11] for example, for single-molecule force measurements,[12] fabrication of artificial nanopores,[13] and plasmonics.[14] However, few studies have investigated the folding process or attempted to control it. The melting of a DNA origami rectangle adsorbed on mica was studied using a temperature-controlled AFM.[15] This seminal work posed the problem for the first time, although it did not characterize the melting of DNA origami in solution but the thermodynamics of DNA origami bound to mica. The strong electrostatic forces between these two objects suggest that one should be cautious when extending these

Received: September 22, 2015
Accepted: January 21, 2016
Published: January 21, 2016

DOI: 10.1021/acsnano.5b05972
ACS Nano 2016, 10, 1978−1987

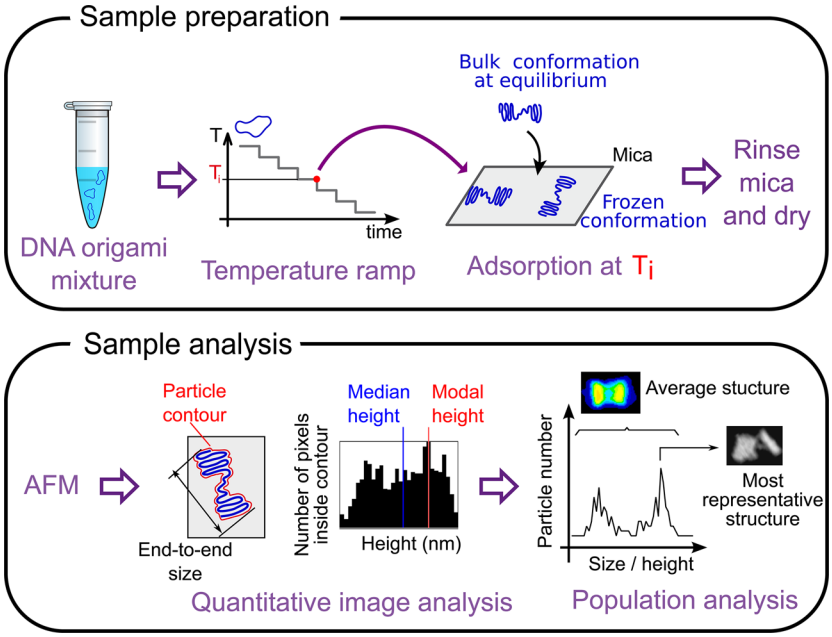

Figure 1. Sketch of the method used to characterize equilibrium origami structures during folding at the single molecule level. Replicate origami solutions (scaffold and staples) were submitted to a slow temperature ramp. At a desired temperature T_i, a piece of mica was immersed in the solution to freeze the equilibrium conformations on its surface by adsorption. Rinsing of adsorbed samples on mica was performed at T_i. After drying, AFM images were acquired. Image analysis yielded particle contours and quantitative data, such as the end-to-end size, and the modal and median height, for every foldamer. Distributions of these parameters were obtained at each temperature, allowing extraction of the average and the most representative structure.

results to DNA origami in free solution.[16] With a temperature-jump method involving a fluorescent DNA binder as read-out, Dietz and co-workers determined that 3D origami folding rate was heavily dependent on the temperature.[17] This work allowed, for instance, reduction of the folding time of 3D origami from 1 week[6] to 2 h,[17] indicating that fundamental thermodynamic studies may have a major influence in technological processes. Recently, insight about the thermodynamics of folding/melting of 2D and 3D origamis was provided by studying the melting curves of DNA origami in bulk using the FRET signal from two fluorescently labeled staples.[9,18] However, none of the aforementioned works has characterized the folding of DNA origami in solution with single-molecule resolution. Such a level of detail is needed for building good theoretical models, which are currently scarce.[19] Recently, a double-scaffold design was used to infer folding pathways from the AFM images of the folded state alone,[20] and single-molecule force spectroscopy was employed to investigate and control folding.[21]

Here, inspired by these seminal works, we used AFM to take snapshots of the folding and melting of DNA origami structures in solution during a temperature ramp. We show evidence of at least six different folding states, with folding nucleation happening at the upper and lower edges of the tall rectangular structure investigated here. As temperature decreases, the nucleation sites grow toward the center of the structure and finally merge to form the fully folded rectangle. A dedicated image analysis procedure allows us to extract a wealth of quantitative data from AFM images. Moreover, we show that the folding pathway can be dramatically modified by changing the concentration of a portion of the staples. Eventually, we demonstrate that data from AFM are consistent with experiments in bulk.

RESULTS AND DISCUSSION

For all the experiments, we used the tall rectangle origami designed by Rothemund[3] as it was previously studied thermodynamically.[15] To gain insight about the folding process at the single-molecule level, we set up a protocol to take AFM snapshots of individual origami particles at different temperatures (Figure 1). To do so, aliquots of a 1:52 nM scaffold/staple solution were heated at 70 °C and then cooled at a rate of 1 °C/15 min. For every temperature, T_i, a piece of mica was immersed in the solution for 1 min to allow the particles to adsorb on the surface. Subsequently, the mica was washed in pure buffer at T_i. The excess salt was removed by rapidly rinsing with water at room temperature. The sample was finally dried and imaged by AFM at room temperature. This method has several advantages. First, the folding process occurs in solution, without the presence of the mica surface. Only when folding has reached thermodynamic equilibrium is the solution put in contact with the mica. As a result, adsorption is not expected to significantly change the folding pathway. Second, sample drying enables us to "freeze" the origami in its equilibrium structure by stopping both the melting of formed structures, that could occur if the mica was imaged in pure buffer, and the hybridization of staples contained in the starting solution.

Folding Proceeds through Five Distinct Intermediates, Some of Them Coexisting at a Given Temperature. First, we used this adsorption/drying method to study the folding process. Figure 2 displays AFM images of single foldamers at different temperatures during cooling. One can visually distinguish at least six distinct states: linear (at 70−69 °C, dark blue arrows), entangled coil (70−63 °C, pink arrows), half-width folded (65−63 °C, green arrows), full-width folded (63−61 °C, red arrows), broken rectangles (63−55 °C, orange arrows), and fully folded structures (59−40 °C, light blue arrows). Several of these structures coexisted at a given

DOI: 10.1021/acsnano.5b05972
ACS Nano 2016, 10, 1978−1987

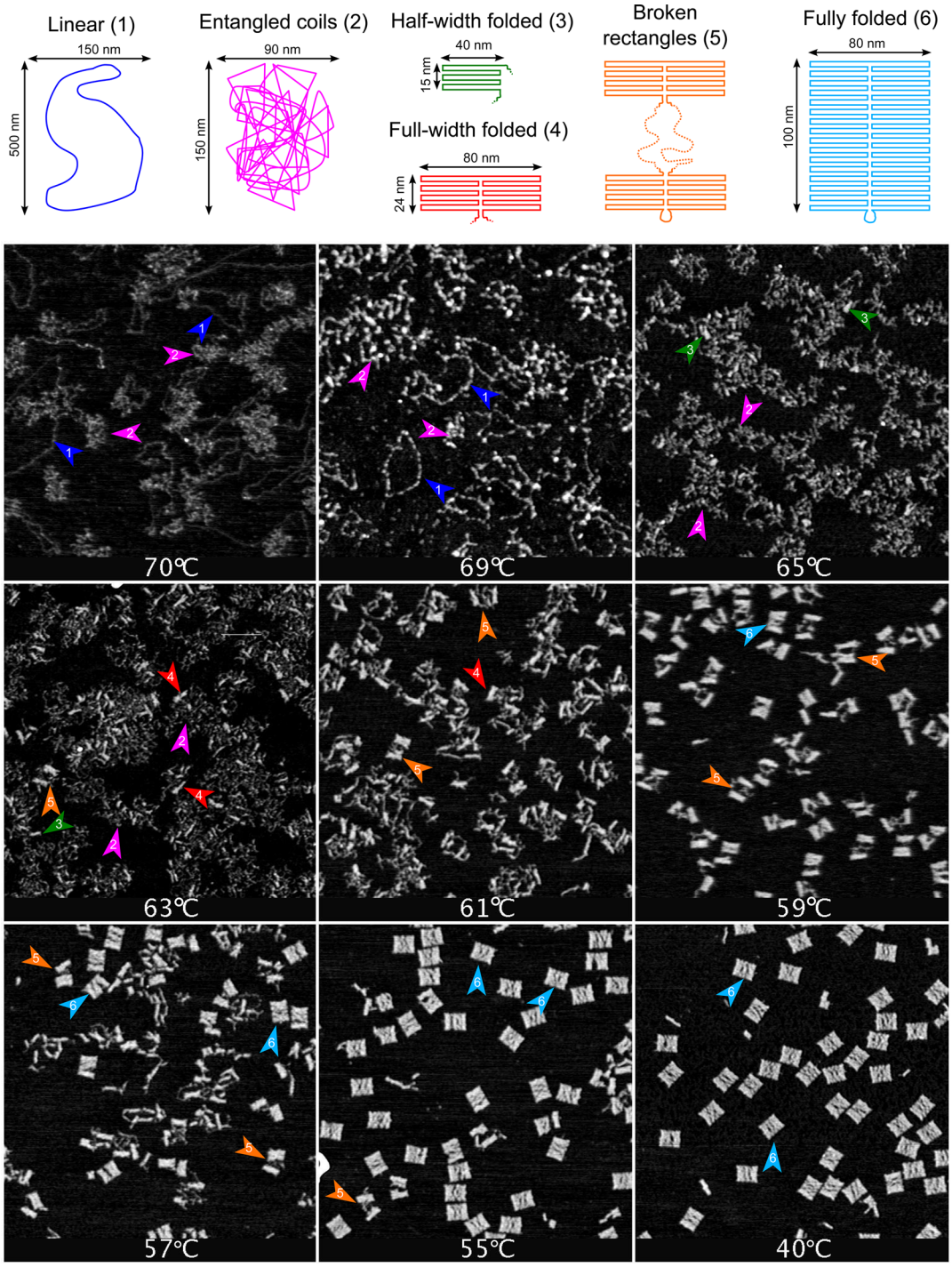

Figure 2. DNA origami structures folding during a cooling ramp of 1 °C/15 min. Scaffold 1 nM, staples 52 nM. (Top) Sketches of the structural types observed. (Bottom) AFM snapshots at different temperatures; each image corresponds to a different sample following the same folding protocol. Colored and numbered arrows indicate structures belonging to the structural types of identical color and number sketched in the top panel. All images are 1.5 × 1.5 μm^2 with a height range of 0−1.3 nm.

temperature, and the fraction of structures that are closer to the folded state increased, as expected, when temperature decreased.

Linear structures were typically 0.4 ± 0.2 nm height and 9 nm in width with lengths up to 960 nm, which we interpret as ssDNA portions of the M13 scaffold that have been stretched during sample drying[22] and probably do not exist in solution. However, they indicate coil configurations that are less strongly held together in solution than entangled coils. Entangled coils had typical dimensions of 150 × 90 nm^2 and were 0.5 ± 0.2 nm high, which is compatible with ssDNA. The first clear structuration was observed at 65 °C: small rectangular portions that may reach 36 × 15 nm^2 across and 1.2 nm high were identified with half-width folded portions of the origami (from the border to the central seam). As the temperature decreased the number of large rectangles increased, as well as their size, 72 × 24 nm^2 at 63 °C and 72 × 34 nm^2 at 61 °C. We identify them as full-width folded portions of the upper or lower part of the

DOI: 10.1021/acsnano.5b05972
ACS Nano 2016, 10, 1978−1987

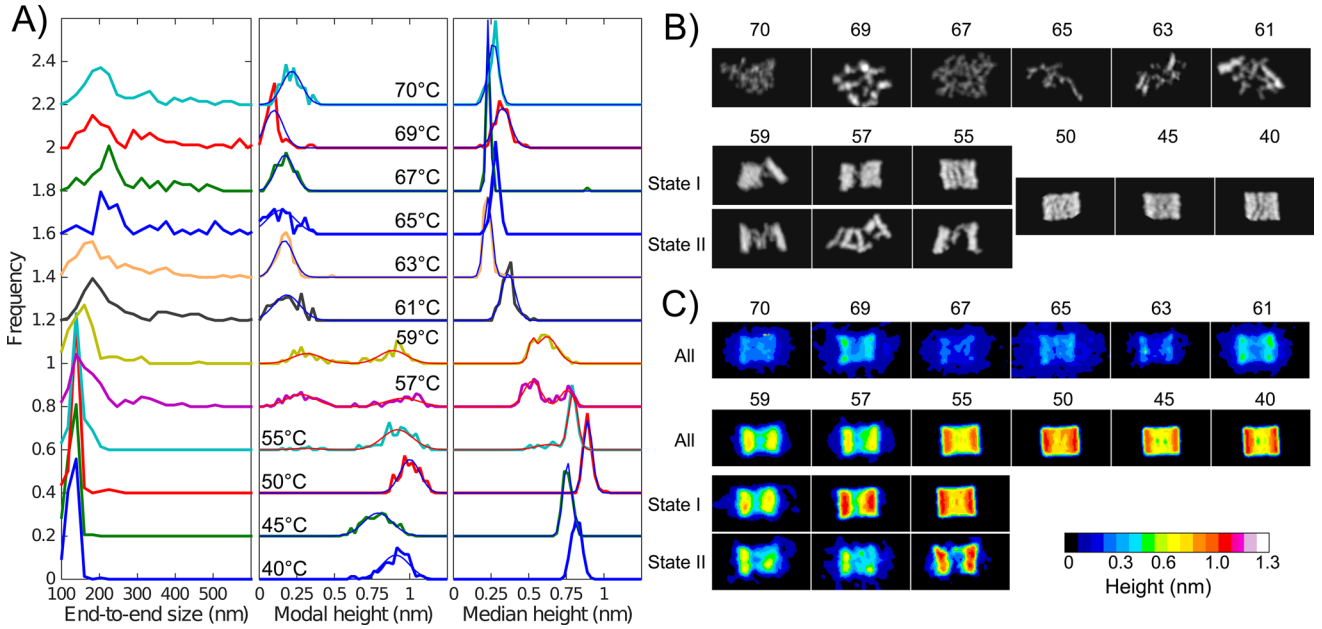

Figure 3. Population analysis of an ensemble of DNA origami particles folding while cooling into a tall rectangle. (A) Histograms of the end-to-end length, the modal height, and the median height of particles extracted from the whole field of view ($3 \times 3\ \mu m^2$) of the images in Figure 2 (see Figures S1 and S2) at different temperatures; plots are offset for clarity. Thin blue and red lines correspond to single and double Gaussian fits, respectively. Between 50 and 150 particles were analyzed for each temperature. (B) AFM images of representative particles close to the maxima of the median height distribution and (C) average AFM images at each temperature. States I and II correspond to the two populations found in the range 55−59 °C. Images are $146 \times 88\ nm^2$. Cooling rate 1 °C/15 min.

rectangle running from the left to the right border across the central seam. Among them, we distinguished either full-width folded or broken rectangle structures, where two full-width folded portions were held together by a short unstructured region. At 59 °C, a majority of particles displayed a broken rectangle structure and at least one was almost perfectly folded. At 57 and 55 °C there was a mixture of broken and fully folded rectangles, the former being the majority at 57 while the later dominated at 55 °C (Table S1). Between 50 and 40 °C, images were practically indistinguishable (Figure S1 and Figure 2), and no partially folded structures were observed. At these temperatures, 85% of the particles folded without defects, 5% displayed large holes up to 1/2 of the tall rectangle surface, and 10% were rectangular particles smaller than 1/4 of the surface of the rectangle.

The full-width folded and broken rectangle structures are particularly interesting. The folded structures appeared always on the top and bottom ends of the tall rectangle, and not in the middle, indicating that folding is not random but starts at well-defined positions of the structure. This result is in agreement with the simulations of Song *et al.*[15] who reported that the calculated melting temperatures of the staples are significantly higher on the top and bottom ends of the tall rectangle. Moreover, their simulation predicted a region of $24 \times 35\ nm^2$ on the bottom left of the rectangle with a particularly high (>63 °C) melting temperature. This region is compatible with the half-width folded structures observed here at 65 and 63 °C. Our results are also in agreement with the recent study of Dunn *et al.*[20] that confirmed that DNA origami folding is highly cooperative and found that early connections (due to staples with high melting temperatures) strongly influenced the folding pathway.

Our data show that little folding happened above 63 °C, suggesting that these temperatures are not necessary for correct folding. To test this, we heated an origami solution at 95 °C, and we followed the same cooling ramp as in Figure 2 except that we skipped the initial part by cooling the sample rapidly to temperature T_i at 1 °C/0.2 s prior to normal cooling at 1 °C/15 min down to 40 °C. Interestingly, we obtained well-formed rectangles down to T_i = 57 °C (Figure S10), a first indication that the folding process is under thermodynamic rather than kinetic control. In a more practical perspective, it shows that our method can be used to identify the temperature where critical folding events occur and therefore significantly simplify the origami formation protocol by focusing the cooling procedure to the range of temperatures where folding takes place.[17]

Quantitative Analysis of the Folding Process. Second, to gain quantitative insight into the folding process, we used a segmentation algorithm to detect and analyze individual particles in the AFM images (see the Methods). Our segmentation procedure succeeded to detect individual particles at 59 °C and below (Figure S1). Above this temperature, the density of adsorbed particles was too large for distinguishing individual structures (Figure S2), and lowering it would result in poor sampling statistics at lower temperatures. To quantify the structural changes of these particles during folding we chose three parameters: the maximum end-to-end size and the modal and the median height (Figure 3A). Note that both heights were calculated by taking into account all pixels within the perimeter of the particle, and thus, holes were counted (Figure 1). Histograms of the end-to-end size (in the following noted size) displayed five distinct shapes, which is consistent with the six structures detected by visual inspection. As one may expect, the modal size and the width of the distribution decreased during cooling. The modal size decreased from 210 ± 10 nm at high temperature until it stabilized at 140 ± 10 nm at 57 °C, in

DOI: 10.1021/acsnano.5b05972
ACS Nano 2016, 10, 1978−1987

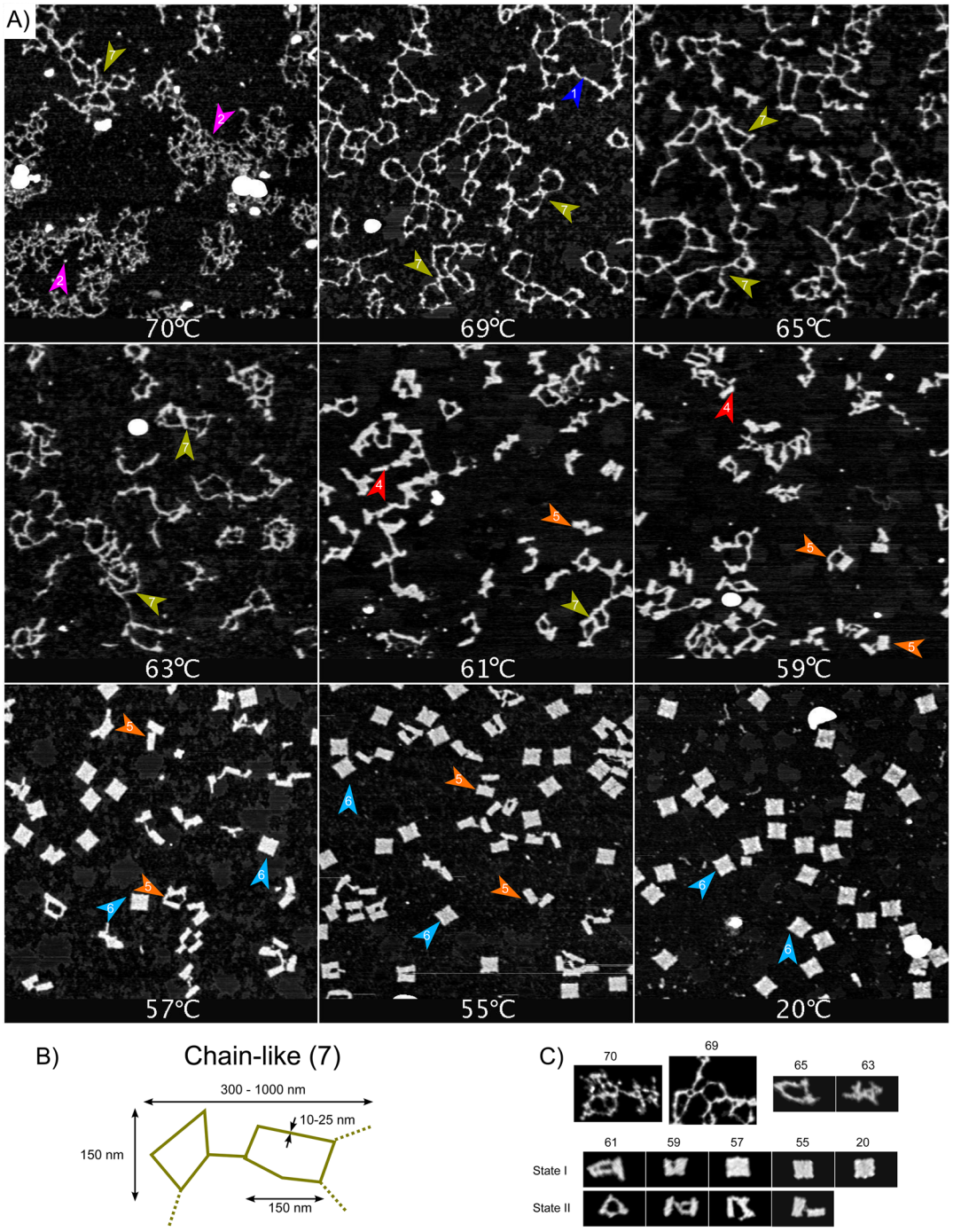

Figure 4. DNA origami structures melting during a heating ramp of 1 °C/10 min. (A) AFM snapshots at different temperatures; each image corresponds to a different sample following the same melting protocol. The images are displayed from high to low temperature to facilitate comparison with Figure 2. Colored and numbered arrows indicate structures belonging to the structural types of identical color and number sketched in Figure 2 and panel B. All images are 1.5 × 1.5 μm^2 with a height range of 0−1.3 nm. (B) Sketch of a new structural type observed during heating. (C) AFM images of representative particles close to the maxima of the median height distribution. Images are 146 × 88 nm^2 except 70 and 69 that are larger but drawn at the same scale.

agreement with the diagonal length of 128 nm expected for the folded tall rectangle. The width of the distribution further decreased until 50 °C, where it remained unchanged and equal to 10 nm. This trend is in agreement with the aforementioned qualitative observations. In contrast with the size distributions, the histograms of the modal height showed only two peaks suggesting that folding is a two-state process. However, this picture is incomplete because the modal height is very sensitive to the existence of holes inside a particle. Indeed, the two peaks should be considered as a signature of the existence of holes within a particle, 0.15 nm indicating some holes and 0.9 nm no holes. In any case, the modal height clearly indicated that in the range 59−55 °C, at least two distinct states coexisted. The histograms of the median height, less sensitive to the existence of holes, revealed at least four states along the folding pathway, at 0.3, 0.4, 0.5, and 0.8 nm (Figure S12).

DOI: 10.1021/acsnano.5b05972
ACS Nano 2016, 10, 1978−1987

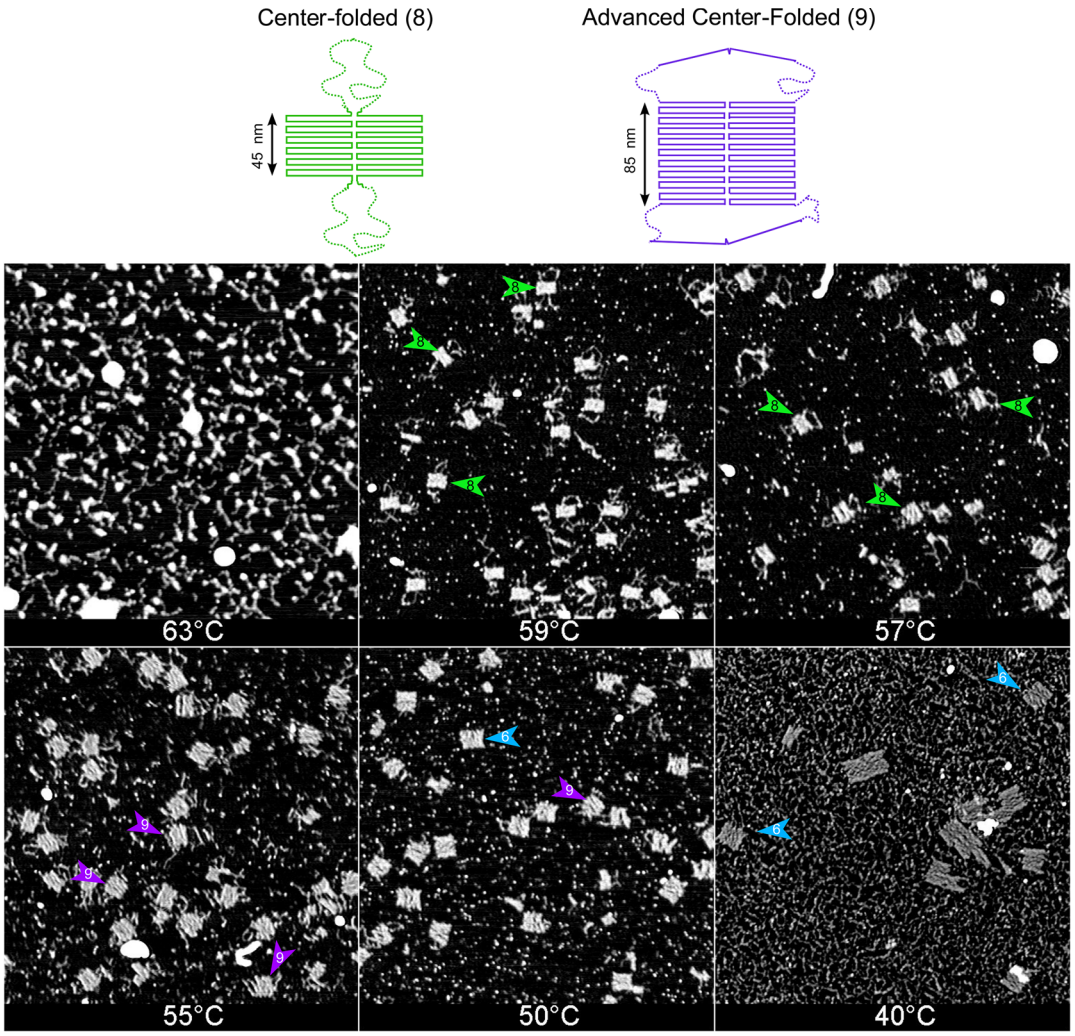

Figure 5. Folding pathway can be controlled by changing the relative concentration of staples. DNA origami structures folding during a cooling ramp of 1 °C/30 min. Scaffold 1 nM, edge staples 1.2 nM, central staples 670 nM. Top: sketches of the new structural types observed. Bottom: AFM snapshots at different temperatures. Colored and numbered arrows indicate structures belonging to the structural types of identical color and number sketched in the top panel and in Figure 2. All images are 1.5 × 1.5 μm^2 with a height range of 0−1.3 nm.

From these data, it is possible to select single particles that best represent the folding process at each temperature. To do so, we fitted the modal and median height distributions to single and double gaussians to find their local maxima. We then looked for particles for which both heights were within 5% of the height corresponding to these maxima. Figure 3B displays, for each temperature, a set of most representative foldamers selected by this method. In the range 59−55 °C, two distinct states were associated with the two maxima observed in the height histograms. We have called these different sets of structures states I and II, and we note that state I at two different temperatures does not necessarily correspond to the same structure. This analysis confirmed the qualitative picture of folding provided above. The most likely foldamers at every temperature were entangled coils (70−65 °C), half-width folded particles (63 °C), full-width folded particles (61 °C), a mixture of two types of full-width folded and broken rectangle particles (59−57 °C), a mixture of broken rectangles and fully folded particles (55 °C), and fully folded particles (50−40 °C). A complementary way of representing these data is to average, at each temperature, the particles after aligning them using an image registration algorithm (Figure 3C) against a prototypical rectangle particle at 40 °C. This procedure is thus biased toward finding average rectangular shapes, as one notices when comparing averages at 69 and 61 °C that look very similar, although whole-field AFM images appear significantly different to the eye (Figure 2). As a result, average images were more informative at lower temperatures where rectangular shapes were more apparent. In particular, they captured well the transition between 61 °C, where full-width folded structures were majority, to 59 °C, where broken rectangles became predominant. Moreover, average particles for states I and II at 57 and 55 °C, clearly showed the existence of two different folding states at these temperatures. In summary, the qualitative and quantitative analysis of AFM images are consistent and quantitative analysis provided statistically significant measures of the structural intermediates that were essential to build up a coherent picture of the folding pathway.

Melting and Folding Pathways Differ at High Temperature. Third, we used our method to investigate the melting pathway of prefolded DNA origamis. Figure 4 displays AFM images of single foldamers at different temperatures during heating. At first sight, two aspects are visually striking when comparing these images with those in Figure 2: the folded

DOI: 10.1021/acsnano.5b05972
ACS Nano 2016, 10, 1978−1987

rectangles corresponding to the melting experiment do not display the weaving internal structure seen in Figure 2, and they look like squares instead of rectangles (they are 80 × 90 nm^2 (±5 nm) instead of 80 × 100 nm^2). These two observations are consistent, the less the horizontally running helices are bound to each other, the more the internal crossovers of the origami should become apparent, resulting in an enlargement of the dimensions along the vertical axes. We have observed a 10% variability in the size of the tall rectangles for experiments performed in different days and found (74 ± 7) × (88 ± 9) nm^2 (one standard deviation, Figure S5). In contrast, the variability is negligible for experiments performed the same day (Figures S6–8). Absolute particle sizes given in this work have thus to be taken with 10% precision, and as a consequence, the folded rectangles in Figures 2 and 4 are identical within experimental precision. Although the folding protocols in the folding and melting experiments were different (see the Methods), we did not observe a correlation between the size and the folding protocol (Figure S5). We thus hypothesize that these changes in shape may come from some parameters that were not controlled in our experiment, especially humidity, and that may influence the adsorption of the sample onto the mica. We conclude that this variability did not influence, within experimental precision, the observed folding state at each temperature.

The data in Figure 4 show that the melting pathway was the reverse of the folding one until 61 °C: the central part of the rectangle melted at a lower temperature than the edges. In this range of temperatures, melting occurred 2 °C above folding (Figure S11), a hysteresis compatible with melting curves of the bulk obtained using absorbance[23] or fluorescence (Figure S13). However, this difference is within the 2 °C experimental precision of our method. In contrast, above 61 °C the folding and melting pathways strongly differed: a new type of structure, called chainlike, was observed (Figure 4B). These chainlike structures reached 1 μm across and were formed of links about 150 nm long. The number of links per particle clearly increased from 63 to 69 °C, in agreement with a progressive unwinding of dsDNA. At 70 °C, we observed a mixture of these chainlike structures together with entangled coils, indicating that at very high temperature the chainlike structures were disrupted. This high-temperature hysteresis was not observed in melting curves of the bulk recorded using a fluorescent DNA intercalator (Figure S13), indicating that the states observed at high temperature for folding and melting, although structurally very different, had a similar number of base pairs. Taken together, these results suggest that chainlike structures are out of equilibrium and correspond to single-stranded M13 loops connected by sets of staples forming dsDNA links with very low dissociation rates (<0.025 min^{-1} in the range 65–69 °C).

Folding Pathway Can Be Controlled by the Relative Concentration of Staples. Fourth, we used the knowledge extracted from the previous experiments to try to control the folding pathway. As we have seen, the folding nucleation sites appeared to be thermodynamically controlled and corresponded to regions having higher melting temperatures, T_m. To test this hypothesis, and taking into account that T_m depends on the concentration for a bimolecular reaction (see SI section 8), we folded the tall rectangle with different relative concentrations of the staples. Figure 5 shows AFM images of the folding process when the concentration of the central and border staples was changed from 52 nM to, respectively, 670 and 1.2 nM. Under these conditions, the folding pathway was dramatically changed and proceeded this time from the center toward the edges. Center-folded structures bearing a 72 × 45 nm^2 double-stranded rectangular region at the center of the structure were observed at 59 °C. This region increased its size to 72 × 85 nm^2 to form an advanced center-folded structure at 55 °C. At 40 °C, normal rectangles were observed on top of a rugged surface, probably due to staple adsorption. Finally, the onset of folding was shifted from 63 to 59 °C, a trend that was also observed in bulk (Figure S14). These results confirm that the folding pathway is controlled thermodynamically and that the nucleation sites correspond to the staples with the highest melting temperature. They moreover open the way to the design of nanostructures that could be controlled by the folding pathway.

To understand the effect of staple concentration on the stability of the nucleation site, let us consider the reaction of one staple, S, with the scaffold, T. We suppose that the staple has two identical binding sites and call C the complex of T bound to one binding site of the staple, D the complex bound to two staples S, and O the well-folded nucleation site where one staple binds at its two sites. In the absence of cooperativity we can write

$$\mathrm{S} + \mathrm{T} \overset{K_1}{\rightleftharpoons} \mathrm{C} \tag{1}$$

$$\mathrm{C} + \mathrm{S} \overset{K_1}{\rightleftharpoons} \mathrm{D} \tag{2}$$

$$\mathrm{C} \overset{K_2}{\rightleftharpoons} \mathrm{O} \tag{3}$$

where K_i is the corresponding equilibrium constant. When the total concentration of staples S_0 is low, we can neglect reaction 2 and the equilibrium concentration of nucleation site, O, scales as $O \sim K_1 S_0$, which is related to T_m. When the staple concentration is in excess, O increases with S_0 only if $K_1 S_0 < 1$. For $K_1 S_0 > 1$, reaction 2 competes with reaction 3 (SI section 8). In other words, decreasing the concentration of the edge staples to 1.2 nM decreases the stability of edge nucleation sites, and increasing the concentration of central staples to 670 nM increases the stability of central nucleation sites as far as $K_1 S_0 < 1$. Our observations suggest that both conditions applied: the increase of the central staples increased the folding temperature of the central region from 55 to 59 °C while the decrease of the edge staples decreased folding temperature of the edges from 61 to 55 °C.

Single-Molecule and Bulk-Folding Experiments Agree. Finally, we checked that the folding pathway drawn from single-molecule data was in agreement with data acquired using standard bulk techniques. To do so, following ref 17, the extent of the origami folding reaction was followed using a fluorescent DNA binder. In these bulk experiments, to increase the signal, the scaffold concentration was 10-fold (10 nM) that of AFM experiments, while the staple concentration remained unchanged (52 nM). For the bimolecular reaction of a scaffold with a staple to form a dsDNA, one expects the extent of the reaction to be controlled by the highest concentration (here the staples). As a result, the 10-fold increase in scaffold concentration should induce negligible changes. Figure 6 shows folding curves corresponding to the median height from AFM data and to fluorescence for bulk experiments (see also Figure S10). Their good agreement is remarkable, indicating that our method, despite relying on an adsorption step, does provide representative snapshots of the folding pathway in bulk. The folding temperatures are 59 and 61.5 °C

DOI: 10.1021/acsnano.5b05972
ACS Nano 2016, 10, 1978–1987

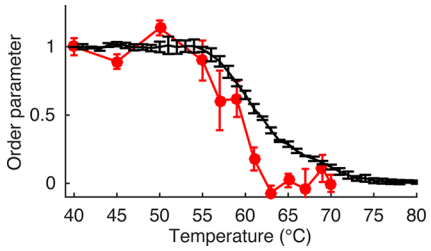

Figure 6. Single-molecule and bulk measurements are in good agreement. Folding curves with the AFM method described here (red disks) and with a standard macroscopic method relying on the fluorescence of a DNA binder[17] (black line). The order parameter for AFM data is the average of the median height for either folding. The order parameter for macroscopic data is the fluorescence of an origami solution minus that of a staples solution during melting. Staples 52 nM, scaffold 1 nM for AFM, and 10 nM for bulk.

for AFM and bulk, respectively. The gap between the two techniques is lower at high and medium folding, 1−2 °C, than at low folding, 4−7 °C. There are three reasons that may explain this difference. First, the presence of the fluorescent binder is reported to stabilize dsDNA structures by 1−2 °C.[24,25] Second, the bulk technique is proportional to the concentration of dsDNA, while AFM is sensitive to the formation of structures large enough to be detected (typically 10 nm). Moreover, the order parameter chosen here, the median height, particularly suffers this bias, as visual inspection of AFM folding data at 65 °C (Figure 2) indicates that some folding has already occurred while the median histogram (Figure 3) does not show any changes. This feature suggests that the bulk experiment will better detect structural changes at low folding while the AFM one will do so for higher folding values, in agreement with the data. Finally, during sample preparation some uncontrolled cooling could occur, especially at high temperatures, although our protocol was designed to minimize these problems (Figure 1 and SI section 10). In contrast with our data, when the tall rectangle was adsorbed on mica and its mechanism studied *in situ* by AFM[15] folding could not be obtained and melting yielded a significantly higher melting temperature. As expected, the interaction between the origami and the mica surface in those experiments over-stabilized the folded state, especially at low folding.

CONCLUSION

In summary, we have developed a method to analyze a large population of origamis, during their folding, that combines, for the first time, statistical analysis on the ensemble and single-molecule resolution. It relies on freezing the conformation of hundreds of individual origamis by adsorption on a mica surface at each temperature of the folding or melting protocol. We have proposed an automated image analysis procedure allowing to extract, for each temperature, the statistical distribution of morphological traits (length, height), an average morphology as well as the most representative one. We think that such a method will be useful not only for or a better understanding of DNA origami folding and other highly complex self-assembly processes (*e.g.*, DNA-mediated particle assembly) but also to quantitatively characterize and compare the performance of emerging methods in DNA nanofabrication, where a simple eye inspection of arbitrarily chosen structures at equilibrium is not enough. For instance, in this work we have used this method to analyze the folding pathway of rectangular DNA origamis with single-molecule resolution. For this particular morphology, we have identified well-defined intermediates corresponding to equilibrium structures and shown that, under standard conditions, folding occurred from the edges to the center, while melting processed through a reverse pathway. In a practical perspective, this method can be used to determine temperatures leading to reproducible structures at equilibrium with peculiar morphologies that are different from the fully folded one at room temperature. We have shown that it can also be exploited to optimize the folding protocol by focusing on the cooling procedure where folding actually takes place, resulting in a gain in robustness (fewer intermediate steps) and time (the folding protocol can be significantly shortened). We thus anticipate this method to be useful not only to optimize fabrication procedures but also for troubleshooting analysis of misfolded origamis. However, the interest in our method is not limited to highly resolved inspection of origami morphologies as a function of temperature. It has allowed us to extract general and new information on the folding pathway of DNA origamis. First, we have demonstrated that folding occurs under thermodynamic control, making DNA origami a particularly reliable tool for building reproducible structures by bottom-up assembly. Second, we have shown that the pathway is primarily defined by the distribution of the melting temperature of staples bound to the scaffold, the origamis folding from high to low melting temperature area. One way to modify the melting temperature distribution consists of changing the sequence of the staples, but this implies a complex adaptation of the scaffold/staple sequence composition for each given structure. In this work, we have demonstrated an experimentally straightforward alternative to affect the melting temperature profile along the folded origami structure without modifying the sequence of neither the scaffold nor the staples. By simply changing the concentration ratio of staples, we have shown that we can increase or decrease the melting temperature of a set of target staples, resulting in a direct control of the origami folding pathway. This constitutes an interesting method to rationally design DNA nanostructures that can be actuated by temperature, with well-defined dynamic morphological responses at predefined positions. Overall, by bringing both a powerful tool of DNA nanostructure analysis and new information on the DNA origami folding pathway, we think this work will contribute to the rationalization of current and future methods to generate highly organized, morphologically sophisticated and dynamically addressable nanostructures generated according to DNA base pairing rules.

METHODS

Sample Preparation. All AFM experiments were performed with a solution of 1 nM of M13mp18 (NEB) in TAE 1X and 12.5 mM magnesium acetate buffer together with the "Tall Rectangle" staples, the sequences of which can be found in Figure S38 of the Supporting Information of ref 3. For standard conditions, we used 52 nM of each of the staples. For Figure 5, we used a mixture of 1.2 nM of the outermost row staples (four on the northern edge and four on the southern edge; the sequences are provided in the SI) and 670 nM of the nine rows of central staples. In all cases the west and east edge staples were not added to minimize the stacking interaction between folded structures on the mica surface. Aliquots (150 μL) of this origami solution were distributed in 500 μL tubes. The same number of aliquots of pure buffer were also prepared.

Temperature-Ramping Protocol. Origami and buffer solutions were subjected to a thermal ramp in a Peqstar 2× thermocycler (Peqlab). For the folding experiment, the ramp consisted of an initial

DOI: 10.1021/acsnano.5b05972
ACS Nano 2016, 10, 1978−1987

10 min long step at 95 °C followed by a decrease of 1 °C every 15 min from 70 to 40 °C. For the melting experiment, we first prepared the fully formed origami with a standard protocol (10 min at 70 °C, followed by a decrease of 1 °C every 2 min from 70 to 40 °C) followed by a 10 min long step at 40 °C, a fast increase of 1 °C every 2 min from 40 to 55 °C, and then a slower increase of 10 min/°C until 70 °C. In both cases, for a given temperature, a *ca.* 3 ×5 mm^2 piece of mica cut with scissors was freshly cleaved and immersed in the origami solution at the end of the step for 1 min. Immersion of a cold piece of mica inside a hot solution is expected to induce a negligible temperature change (SI section 10). The mica was then quickly taken out and dipped into a buffer solution having the same temperature for 30 s. The mica was subsequently removed from the buffer, delicately washed with 1 mL of Milli-Q water at room temperature (Figure S9), quickly dried under a compressed air stream and stuck on a metal disk using double-sided tape prior to AFM observation.

AFM Imaging. AFM images were acquired using an Agilent Technologies 5100 scanning probe microscope in tapping mode in air. We used AppNano FORT silicon probes with 43−81 kHz nominal frequency and 0.6−3.7 N/m force constant. The amplitude set point was typically 15−20 V and the scan rate 1.5 lines/s. Raw AFM images were baseline corrected using Gwyddion: we sequentially performed a "Flatten base" and a "Line-wise sliding median correction" until the corrected image did not change further (in our hands three "Flatten base" and two "Line-wise sliding"). The "Flatten base" subtracts a global polynomial fit to the image excluding aberrant data points. The "Line-wise sliding" calculates the median of the pixel intensity of a line and its adjacent line and shifts the pixels such that the medians are equal. This process is carried on the entire image. Note that the relative heights within a sample preparation are consistent but absolute values (for example de height of dsDNA) from sample to sample may vary by ±0.2 nm. Because our AFM images were obtained on dried samples the height of dsDNA was 1.2 nm instead of 2 nm.

Image Segmentation. The 32-bit corrected AFM images were segmented using a semiautomatic custom-made procedure in ImageJ 2.0. First, images were binarized using an optimal threshold determined manually. To do so, every image was segmented with a systematic range of thresholds in 0.05 nm steps, the outline of the detected particles was overlaid over the AFM image and the optimal threshold was determined visually. This threshold depended on the height of the particles in the sample and thus on the temperature of the folding experiment. The optimal thresholds (in nm) for the folding experiment were 0.5 for $T \leq 50$, 0.3 for $55 \leq T \leq 59$, 0.2 for $T = 61$ and 0.1 for $T \geq 63$, where T is the temperature (°C). The thresholds for the melting experiment were identical except for $T \geq 63$ where the threshold was 0.15 nm. Binary images were eroded once and dilated twice, except for $T \leq 50$ were erosion was done twice followed by three dilations. Subsequently, for every image, particles were detected using the function "Analyze Particles". Particles smaller than 4.7×10^3 nm^2 were discarded for all samples, and particles larger than 1.6×10^4 nm^2 were discarded for $T \leq 55$, *i.e.*, where origami were almost fully formed, to remove particles resulting from two rectangles touching each other. For comparison, the area of a tall rectangle was 8×10^3 nm^2. Particles touching the borders of the image were discarded and no constrain on the circularity of the particles was used. This procedure is available in SI section 11.

Fluorescence Melting Curves. Melting curves of rectangular origami in bulk were obtained through a method adapted from ref 17. The scaffold/staples concentration was 10:52 nM. Experiments were performed in the same buffer as AFM experiments supplemented with 160 nM SybrGreen I; *i.e.*, there is less than 1 SybrGreen molecule per 400 bp. The sample was heated to 90 °C and cooled at a rate of 1 or 1 °C/30 min. Control experiments containing the scaffold, and the staples alone were also performed. The order parameter was obtained by subtracting staples fluorescence from origami fluorescence and normalizing.

ASSOCIATED CONTENT

Supporting Information

The Supporting Information is available free of charge on the ACS Publications website at DOI: 10.1021/acsnano.5b05972.

Figures S1−S14, Table S1, a discussion of the effect of staple concentration on melting temperature, and an evaluation of the thermal effect (PDF)

Matlab and ImageJ routines for image segmentation (ZIP)

Sequences of staples used (XLS)

AUTHOR INFORMATION

Corresponding Author

*E-mail: andre.estevez-torres@upmc.fr.

Notes

The authors declare no competing financial interest.

ACKNOWLEDGMENTS

This work was funded by the European Comission FET-STREP under award Ribonets and by the ANR jeunes chercheurs program under award Dynano. We thank X. Tassart for preliminary experiments and J. C. Galas, A. Zadorin, A. Genot, Y. Rondelez, and J.-P. Aimé for insightful discussions.

REFERENCES

(1) Seeman, N. C. Nucleic-acid Junctions and Lattices. *J. Theor. Biol.* **1982**, *99*, 237−247.

(2) Chen, J.; Seeman, N. C. Synthesis from DNA of a Molecule with the Connectivity of a Cube. *Nature* **1991**, *350*, 631−633.

(3) Rothemund, P. W. K. Folding DNA to Create Nanoscale Shapes and Patterns. *Nature* **2006**, *440*, 297−302.

(4) Han, D.; Pal, S.; Nangreave, J.; Deng, Z.; Liu, Y.; Yan, H. DNA Origami with Complex Curvatures in Three-Dimensional Space. *Science* **2011**, *332*, 342−346.

(5) Pinheiro, A. V.; Han, D.; Shih, W. M.; Yan, H. Challenges and Opportunities for Structural DNA Nanotechnology. *Nat. Nanotechnol.* **2011**, *6*, 763−772.

(6) Douglas, S. M.; Dietz, H.; Liedl, T.; Hogberg, B.; Graf, F.; Shih, W. M. Self-assembly of DNA into Nanoscale Three-dimensional Shapes. *Nature* **2009**, *459*, 414−418.

(7) Dietz, H.; Douglas, S. M.; Shih, W. M. Folding DNA into Twisted and Curved Nanoscale Shapes. *Science* **2009**, *325*, 725.

(8) Andersen, E. S.; Dong, M.; Nielsen, M. M.; Jahn, K.; Subramani, R.; Mamdouh, W.; Golas, M. M.; Sander, B.; Stark, H.; Oliveira, C. L. P.; Pedersen, J. S.; Birkedal, V.; Besenbacher, F.; Gothelf, K. V.; Kjems, J. Self-assembly of a Nanoscale DNA Box with a Controllable Lid. *Nature* **2009**, *459*, 73−76.

(9) Wei, X.; Nangreave, J.; Jiang, S.; Yan, H.; Liu, Y. Mapping the Thermal Behavior of DNA Origami Nanostructures. *J. Am. Chem. Soc.* **2013**, *135*, 6165−6176.

(10) Benson, E.; Mohammed, A.; Gardell, J.; Masich, S.; Czeizler, E.; Orponen, P.; Hogberg, B. DNA Rendering of Polyhedral Meshes at the Nanoscale. *Nature* **2015**, *523*, 441−4.

(11) Endo, M.; Yang, Y.; Sugiyama, H. DNA Origami Technology for Biomaterials Applications. *Biomater. Sci.* **2013**, *1*, 347−360.

(12) Pfitzner, E.; Wachauf, C.; Kilchherr, F.; Pelz, B.; Shih, W. M.; Rief, M.; Dietz, H. Rigid DNA Beams for High-Resolution Single-Molecule Mechanics. *Angew. Chem., Int. Ed.* **2013**, *52*, 7766−7771.

(13) Langecker, M.; Arnaut, V.; Martin, T. G.; List, J.; Renner, S.; Mayer, M.; Dietz, H.; Simmel, F. C. Synthetic Lipid Membrane Channels Formed by Designed DNA Nanostructures. *Science* **2012**, *338*, 932−936.

(14) Kuzyk, A.; Schreiber, R.; Fan, Z.; Pardatscher, G.; Roller, E.-M.; Hogele, A.; Simmel, F. C.; Govorov, A. O.; Liedl, T. DNA-based Self-

DOI: 10.1021/acsnano.5b05972
ACS Nano 2016, 10, 1978−1987

assembly of Chiral Plasmonic Nanostructures with Tailored Optical Response. *Nature* **2012**, *483*, 311−314.
(15) Song, J.; Arbona, J.-M.; Zhang, Z.; Liu, L.; Xie, E.; Elezgaray, J.; Aime, J.-P.; Gothelf, K. V.; Besenbacher, F.; Dong, M. Direct Visualization of Transient Thermal Response of a DNA Origami. *J. Am. Chem. Soc.* **2012**, *134*, 9844−9847.
(16) Pastré, D.; Piétrement, O.; Fusil, S.; Landousy, F.; Jeusset, J.; David, M.-O.; Hamon, L.; Le Cam, E.; Zozime, A. Adsorption of DNA to Mica Mediated by Divalent Counterions: A Theoretical and Experimental Study. *Biophys. J.* **2003**, *85*, 2507−2518.
(17) Sobczak, J.-P. J.; Martin, T. G.; Gerling, T.; Dietz, H. Rapid Folding of DNA into Nanoscale Shapes at Constant Temperature. *Science* **2012**, *338*, 1458−1461.
(18) Wei, X.; Nangreave, J.; Liu, Y. Uncovering the Self-Assembly of DNA Nanostructures by Thermodynamics and Kinetics. *Acc. Chem. Res.* **2014**, *47*, 1861−1870.
(19) Arbona, J. M.; Elezgaray, J.; Aimé, J. P. Modelling the Folding of DNA Origami. *Europhys. Lett.* **2012**, *100*, 28006.
(20) Dunn, K. E.; Dannenberg, F.; Ouldridge, T. E.; Kwiatkowska, M.; Turberfield, A. J.; Bath, J. Guiding the Folding Pathway of DNA Origami. *Nature* **2015**, *525*, 82−86.
(21) Bae, W.; Kim, K.; Min, D.; Ryu, J. K.; Hyeon, C.; Yoon, T. Y. Programmed Folding of DNA Origami Structures Through Single-molecule Force Control. *Nat. Commun.* **2014**, *5*, 5654.
(22) Allemand, J. F.; Bensimon, D.; Jullien, L.; Bensimon, A.; Croquette, V. pH-dependent Specific Binding and Combing of DNA. *Biophys. J.* **1997**, *73*, 2064−2070.
(23) Arbona, J. M.; Aime, J. P.; Elezgaray, J. Cooperativity in the Annealing of DNA Origamis. *J. Chem. Phys.* **2013**, *138*, 015105.
(24) Monis, P. T.; Giglio, S.; Saint, C. P. Comparison of SYTO9 and SYBR Green I for Real-time Polymerase Chain Reaction and Investigation of the Effect of Dye Concentration on Amplification and DNA Melting Curve Analysis. *Anal. Biochem.* **2005**, *340*, 24−34.
(25) Gudnason, H.; Dufva, M.; Bang, D. D.; Wolff, A. Comparison of Multiple DNA Dyes for Real-time PCR: Effects of Dye Concentration and Sequence Composition on DNA Amplification and Melting Temperature. *Nucleic Acids Res.* **2007**, *35*, e127.
(26) Wei, B.; Dai, M.; Yin, P. Complex Shapes Self-Assembled from Single-Stranded DNA Tiles. *Nature* **2012**, *485* (7400), 623−626.

DOI: 10.1021/acsnano.5b05972
ACS Nano 2016, 10, 1978−1987